Adaptive Optics Communications Performance Analysis

M. Srinivasan,[1] V. Vilnrotter,[1] M. Troy,[1] and K. Wilson[1]

The performance improvement obtained through the use of adaptive optics for deep-space communications in the presence of atmospheric turbulence is analyzed. Using simulated focal-plane signal-intensity distributions, uncoded pulse-position modulation (PPM) bit-error probabilities are calculated assuming the use of an adaptive focal-plane detector array as well as an adaptively sized single detector. It is demonstrated that current practical adaptive optics systems can yield performance gains over an uncompensated system ranging from approximately 1 dB to 6 dB depending upon the PPM order and background radiation level.

I. Introduction

NASA currently is planning optical links to support deep-space communications at minimum data rates of 10 Mb/s from Mars to a ground receiver on Earth. A crucial aspect of this effort is the development of strategies to mitigate the effects of high background radiation and atmospheric turbulence on the optical communications link performance. Adaptive optics is one strategy being considered. In this article, the performance of adaptive-optics-aided direct detection of optical communication signals received through atmospheric turbulence is evaluated. Performance is characterized in terms of the uncoded pulse-position modulation (PPM) bit-error rates (BERs) as a function of adaptive optics (AO) complexity and the corresponding gains of adaptive optics systems over nominal reception with no adaptive optics compensation. Detection methods developed in [1] have been applied to this problem—specifically, the use of a photon-counting focal-plane detector array whose elements may be selectively combined to optimize performance, assuming Poisson-distributed signal and background counts.

The effect of atmospheric turbulence upon the optical signal-intensity distribution in the focal plane is twofold: first, small-scale turbulence tends to distort the diffraction-limited point spread function (PSF) and effectively "spread" the signal intensity over a larger area than the diffraction-limited PSF; second, the centroid of the distribution tends to wander in the focal plane, with the extent of the excursions determined by the outer scale of turbulence [2]. This then requires a larger-area photodetector in order to capture the required number of signal photons and achieve the desired level of performance. As the background radiation intensity is assumed to have a uniform distribution over the focal-plane detector, the larger effective detector area containing significant signal energy results in proportionally more collected background photons, and hence degraded communications performance. With adaptive optics,

[1] Communications Systems and Research Section.

The research described in this publication was carried out by the Jet Propulsion Laboratory, California Institute of Technology, under a contract with the National Aeronautics and Space Administration.

however, the distorted focal-plane signal distribution can be reconstructed to some extent, concentrating the signal energy into a smaller area in the focal plane, thus achieving a degree of discrimination against unwanted background interference. The amount of improvement depends upon the complexity of the AO system, which is a function of the number of deformable mirror actuators used to fit to the atmospheric turbulence [3].

II. Performance Analysis

The process of determining communications performance begins with simulating the effect of atmospheric turbulence on the focal-plane signal distribution through the use of Kolmogorov phase screens [3,4]. An atmospheric coherence length r_0 (or Fried parameter) of 7 cm was assumed at the receiver aperture, representing nominal turbulence conditions. A 1-m telescope aperture and 1-Å optical filter around a nominal signal wavelength of 1.064 μm also were assumed. A sequence of AO systems with a varying numbers of actuators, ranging from no actuators (and hence no compensation) to as many as 200 actuators across the pupil diameter, then was simulated. The total number of actuators is approximately the square of the number of actuators across the pupil diameter, but the results here are parameterized by the number across the diameter. The limiting case of no wave-front aberration (no signal distortion) also was determined by computing performance assuming an undistorted diffraction-limited point spread function. In Fig. 1, some examples of the simulated focal-plane distributions are given for a 1-m aperture and 7-cm Fried parameter. Figure 1(a) shows the focal-plane distribution (top view and profile) when no adaptive optics are used, demonstrating the spreading out of the signal intensity with numerous "hot spots." Figure 1(b) contains the focal-plane distribution when an AO system with 9 actuators across the pupil diameter is used, showing the partial reconstruction of the signal core, but significant energy in the

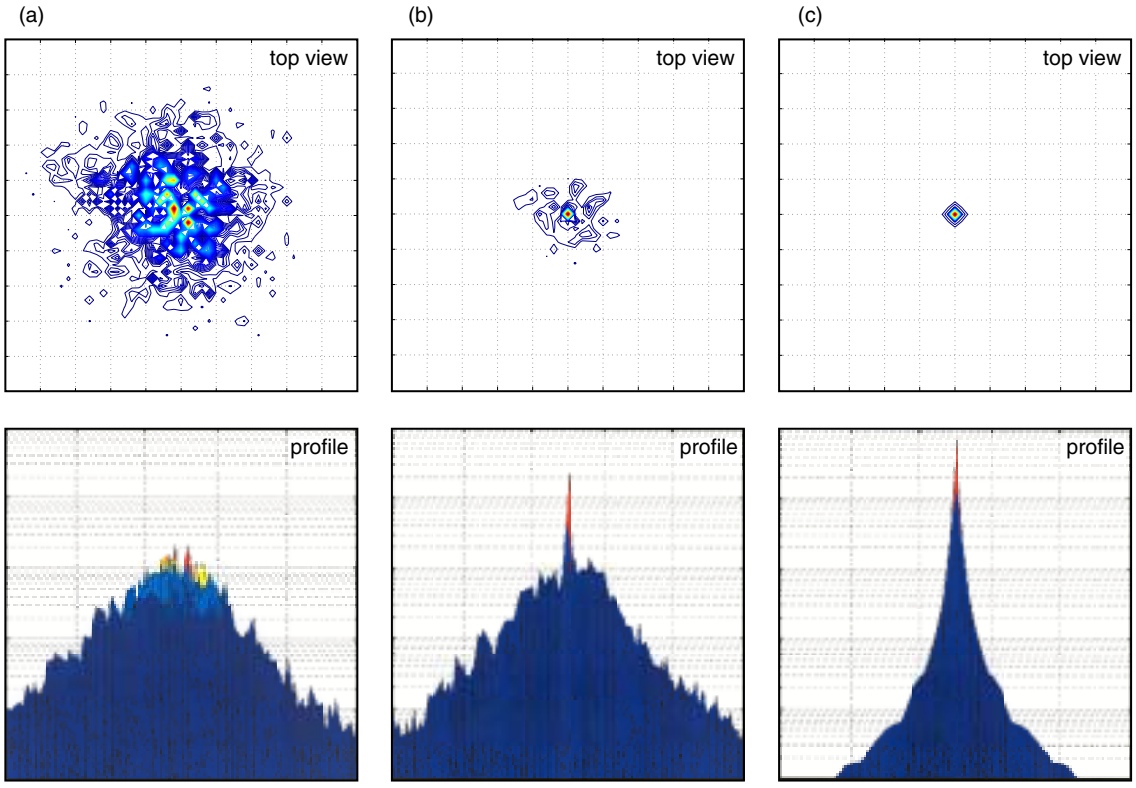

Fig. 1. Focal-plane intensity distributions for a 1-m aperture with (a) no adaptive optics and a Fried parameter of 7 cm, (b) an AO system with 9 actuators across the pupil diameter and a Fried parameter of 7 cm, and (c) no wave-front aberration (diffraction-limited focal-plane distribution).

pedestal or halo surrounding it. In Fig. 1(c), the result of no wave-front aberration is shown, representing the ideal focal-plane signal-intensity distribution. These focal-plane intensities were used to scale the number of signal photons per PPM pulse, n_t, detected over the entire focal plane. For the purposes of this study, it is assumed that n_t is constant from pulse to pulse. Also note that n_t is the total number of *detected* signal photons, and that optical and detection efficiencies have already been incorporated into this number.

The number of background photons per PPM slot, which depends upon the spectral radiance of the noise source in addition to the receiver field of view (FOV), is a key parameter in determining communications performance; therefore, three different values of spectral radiance were assumed, corresponding to vastly different background conditions and environments. Although we consider only uniform background distributions here, which result in uniform background intensity over the focal plane, this assumption is not necessary for the performance-analysis methods described in this article to be valid. The analysis is general enough to allow the determination of receiver performance even if non-uniform background sources are present, as might occur in practice with bright stars in the receiver's field of view or with the limb of a bright planet imaged over the focal plane. In such cases, the same analysis can be applied to determine receiver performance as with the uniform background case; however, performance generally will suffer if intense point sources or bright planetary limbs are observed along with the signal. The values of spectral radiance considered here were (in units of microwatts per square centimeter-nanometer-stearadian)

(1) 0.5, corresponding to 3-km altitude daytime clear sky [5]

(2) 10, corresponding to daytime nominal sea level [6]

(3) 100, corresponding to sunlight scattering from optics [6]

The conversion of these values into the mean number of background photons per PPM slot depends upon the photodetector size, optics and detector efficiencies, the data rate, and the PPM order used. Because the photodetector size is optimized for the number of actuators used in the AO system, the mean number of background photons per slot varies; hence, we provide the background photon levels per diffraction-limited field of view, or pixel, which we denote by Δn_b. At a nominal data rate of 10 Mb/s, the values of Δn_b were calculated to be 4.19×10^{-4}, 8.37×10^{-3}, and 8.37×10^{-2} for 16-PPM for the three different spectral radiance values, respectively. For 64-PPM, the values are 1.57×10^{-4}, 3.14×10^{-3}, and 3.14×10^{-2}, and for 256-PPM the values are 5.23×10^{-5} , 1.05×10^{-3}, and 1.05×10^{-2}. The actual average number of background photons per slot then is calculated from these numbers by summing over the number of diffraction-limited pixels in the detector, which is optimized for the particular operating point being considered and therefore is variable. We further assumed direct photon-counting detection with Poisson output statistics for both the signal fields and the background radiation; the latter case can be justified by the assumption of multimode background fields, as described in [1]. While the background conditions specified here cover a range of operating conditions, mission-specific background values require further validation.

Two methods of photodetector signal processing were considered: one using an adaptive array of detectors and the other using just a single large square detector whose size is optimized with respect to the signal and background photon level. In [1], it was shown that the deleterious effect of atmospheric turbulence could be mitigated by utilizing an array of photodetectors in the focal plane and then processing the outputs of those detector elements in order to minimize the bit-error rate. As shown in [1], the probability of correct detection for PPM is just the probability that the log-likelihood function $\Lambda(T)$ associated with the transmitted symbol exceeds all other log-likelihood functions. Thus, when the qth PPM symbol is sent, a correct decision is made if the log-likelihood function for the qth hypothesis exceeds the log-likelihood function for all other (incorrect) hypotheses: $\Lambda_q(T) > \Lambda_i(T)$ for all $i \neq q$. The log-likelihood function can be expressed as

$$\Lambda_i(T) = \sum_{m=1}^{K} u_m N_m^{(i)} \tag{1}$$

where $N_m^{(i)}$ is the number of detected photon counts in the ith slot of the mth detector of the K-element detector array and u_m is a logarithmic function of the mean number of signal counts per PPM pulse and mean number of background counts per slot, as defined in [1]. In this form, we can see that the log-likelihood function is composed of sums of a random integer number of logarithmic weights from each detector element. The optimum PPM detector thus consists of calculating a logarithmically weighted sum of detector outputs for each hypothesized signal slot and picking the PPM symbol corresponding to the maximum sum. However, the analysis in [1] suggests that detectors observing much more background than signal do not contribute significantly to the error probability, since the outputs of these detector elements are multiplied by weights that are close to zero. This observation leads to a simpler suboptimum decoder concept: list the detector elements starting with the one containing the most signal energy, followed by every other detector ordered according to decreasing signal energy. Compute the probability of error for the first detector element plus background, then form the sum of signal energies from the first two detector elements (plus background for two detector elements), and so on, until the minimum-error probability is reached. Each subset of detectors therefore has weights of "1" applied to the detector elements, while the detector elements not included have weights of "0." The set of detector elements that achieves the minimum probability of error is the best "1-0" detector matched to the signal-intensity distribution. An example of a typical "1-0" detector array is shown in Fig. 2(a).

To reiterate, this strategy is equivalent to partitioning the logarithmic weights into two classes: large weights are assigned the value one, while small weights are assigned the value zero. As shown in [1], this simple partitioning achieves near-optimum performance in low to moderate background environments, but with reduced decoder complexity. Even in high background environments, its performance is only a few tenths of a dB worse than the optimally weighted array.

As an alternative to processing the numerous detector outputs, one may choose simply to use a single large detector encompassing most of the signal energy in the focal plane. The size of this single detector must vary with the signal distribution in the focal plane in order to most effectively capture the signal energy and reject background. This variably sized single detector therefore can be viewed as a detector

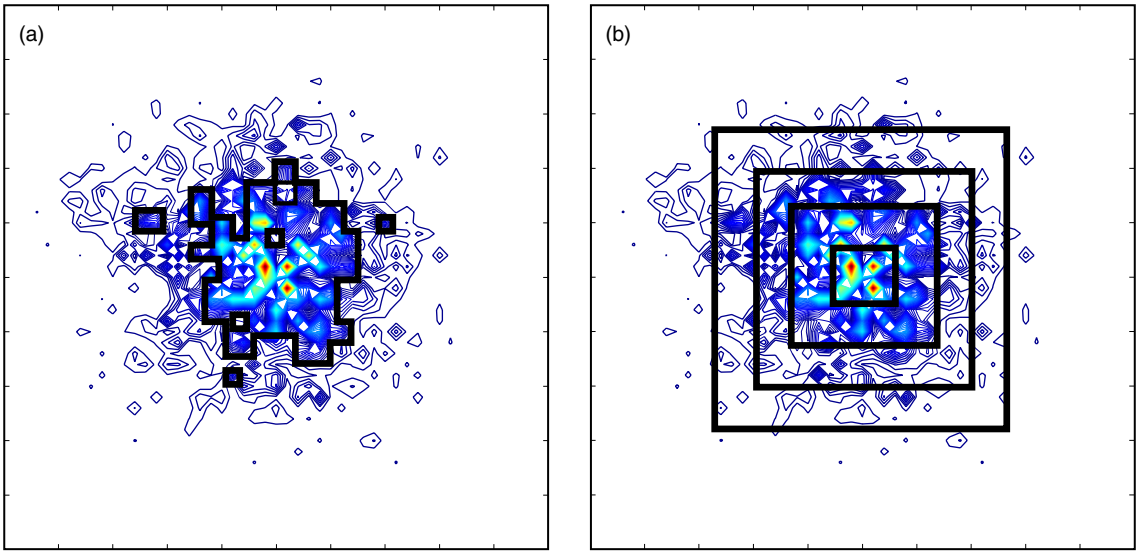

Fig. 2. Focal-plane detector array signal processing methods: (a) near-optimal adaptive subarray and (b) adaptively sized single square detector.

array constrained in its geometry, but it may be implemented through the use of an iris in front of a single large detector in the focal plane or an adjustable zoom lens to spread the signal distribution over the single detector. Here we assume the use of a single square detector centered at the maximum signal intensity point in the focal plane. The dimension of this square detector is adaptively chosen to minimize the probability of bit error for each operating point. The single square detector concept is illustrated in Fig. 2(b).

Upon reception of a PPM symbol frame, the received symbol is detected correctly if the sum of outputs from all selected detector elements over the signal slot exceeds the sum of the selected detector outputs from every other (non-signal) slot. When the array consists of a single detector, the weights can be set to one, and the probabilities then are governed by the Poisson density defined over the integers.

For both the adaptive "1-0" strategy and the single "best" square detector described above, the probability of correct detection can be obtained by assuming constant signal and background intensities over each time slot, yielding the conditional probabilities for the signal-plus-background and background slots, respectively, as

$$p_q(k|H_q) = \frac{(\lambda_s\tau + \lambda_b\tau)^k}{k!} e^{-(\lambda_s\tau+\lambda_b\tau)} \tag{2a}$$

and

$$p_i(k|H_q) = \frac{(\lambda_b\tau)^k}{k!} e^{-\lambda_b\tau} \tag{2b}$$

where $\lambda_s\tau$ and $\lambda_b\tau$ are the average signal and background counts over τ-second signal and background slots, respectively, and are taken over the selected detector subarray or single-detector area, so that they vary over the particular operating point. The probability of correct detection can be determined, using these Poisson densities, as

$$P_M(C) = \sum_{k=1}^{\infty} \frac{1}{M} e^{-\lambda_s\tau} \left(1 + \frac{\lambda_s}{\lambda_b}\right)^k \left\{ \left(\sum_{j=0}^{k} \frac{(\lambda_b\tau)^j}{j!} e^{-\lambda_b\tau} \right)^M - \left(\sum_{j=0}^{k-1} \frac{(\lambda_b\tau)^j}{j!} e^{-\lambda_b\tau} \right)^M \right\} + \frac{e^{-(\lambda_s + M\lambda_b)\tau}}{M} \tag{3}$$

This, in turn, yields the probability of error as $P_M(E) = 1 - P_M(C)$. The resulting error probability then can be evaluated to determine the performance of the AO system under operating conditions of interest.

III. Numerical Results

The performance of the AO system under the various conditions described earlier is presented in Figs. 3 through 14. Figure 3(a) shows the uncoded bit-error rate (BER) as a function of the total number of detected signal photons per signal pulse n_t, for 16-PPM with the background level as specified by the smallest spectral radiance value given earlier in Case (1), yielding 4.19×10^{-4} mean detected background photons per diffraction-limited pixel. The curves are shown for selected values of n, the number of actuators across the pupil to correct wave-front error: $n = 0$, $n = 9$, $n = 31$, and finally the case of no wave-front error. We note that the $n = 9$ AO system only improves the performance of the uncompensated $n = 0$ system by about 0.2 dB at a 0.01 BER, whereas the $n = 31$ AO system results in an improvement of about 1.3 dB, which is about 0.5 dB short of the limiting performance (at

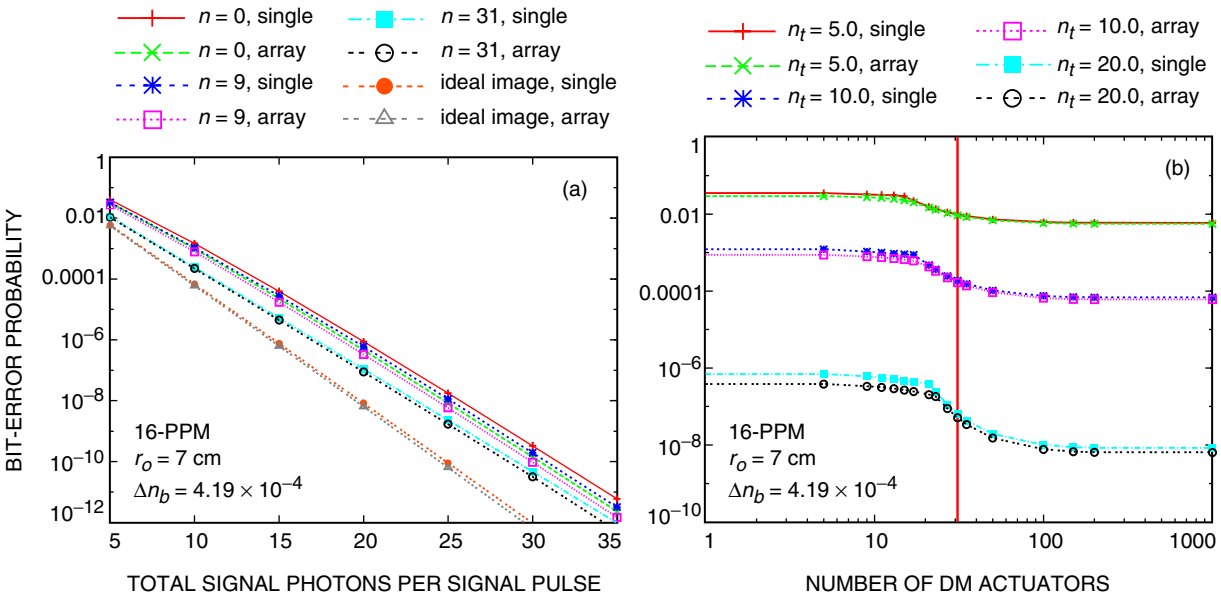

Fig. 3. Bit-error rates for an array detector and a single detector, 16-PPM, background Case (1): (a) BER versus the mean total number of detected signal photons in the focal plane for various AO systems and (b) BER versus the number of DM actuators across the pupil, for specific signal photon levels.

a 0.01 BER) corresponding to no wave-front error. Results are given for both the single detector and the array detector processing schemes, showing that the difference between the performances of the single detector and the array detector is small, becoming insignificant for the higher-complexity AO systems. For example, at a bit-error rate of 10^{-6}, the performance difference between the single detector and the array is about 0.2 dB for the $n = 0$ case, but is reduced to 0.002 dB when there is no wave-front error. This reduction is due to the fact that the improved wave-front correction allows for improved spatial filtering and hence a reduction in background light incident upon the single detector, allowing it to perform as well as the array. Therefore, under the conditions specified here, performance close to the near-optimum 0-1 array may be approached with the single square detector whose size is adjusted to match the signal-field distribution in the focal plane. The implications of this approach for implementation are significant, since the complicated processing of selecting the correct number of possibly disjoint detector elements required for the 0-1 array detector can be replaced with simpler processing applied to a regular subarray, or even with a single large detector element with appropriate zoom optics to achieve the required spatial adaptation as the extent of the PSF changes due to turbulence.

Figure 3(b) shows the same bit-error rates as Fig. 3(a), but now as a function of the number of actuators across the pupil, for the three values of total number of signal photons per pulse of $n_t = 5$, 10, and 20. A vertical line is drawn at a value of $n = 31$ actuators across the pupil, denoting the practical limit of what may be currently implemented in a 1-m telescope. This figure again shows how close the array and single-detector performances are, as well as the degree of improvement afforded by more complex AO systems. We see that the uncoded bit-error rate remains virtually unchanged until an AO system with $n = 17$ or higher is used. As the number of actuators increases, the performance continues to improve until $n = 100$, at which point the curves flatten out again. We also see that more significant gains appear to occur with higher values of n_t. As a practical matter, however, the region of real interest is uncoded BER around 0.01 or higher, which corresponds to a coded BER of 10^{-6} with current coding techniques.

Figures 4 and 5 show the 16-PPM results when spectral radiance Cases (2) and (3) are considered. We observe that, as the amount of background increases, the improvement in performance given by more actuators is greater, and that the difference between the single detector and the detector array also

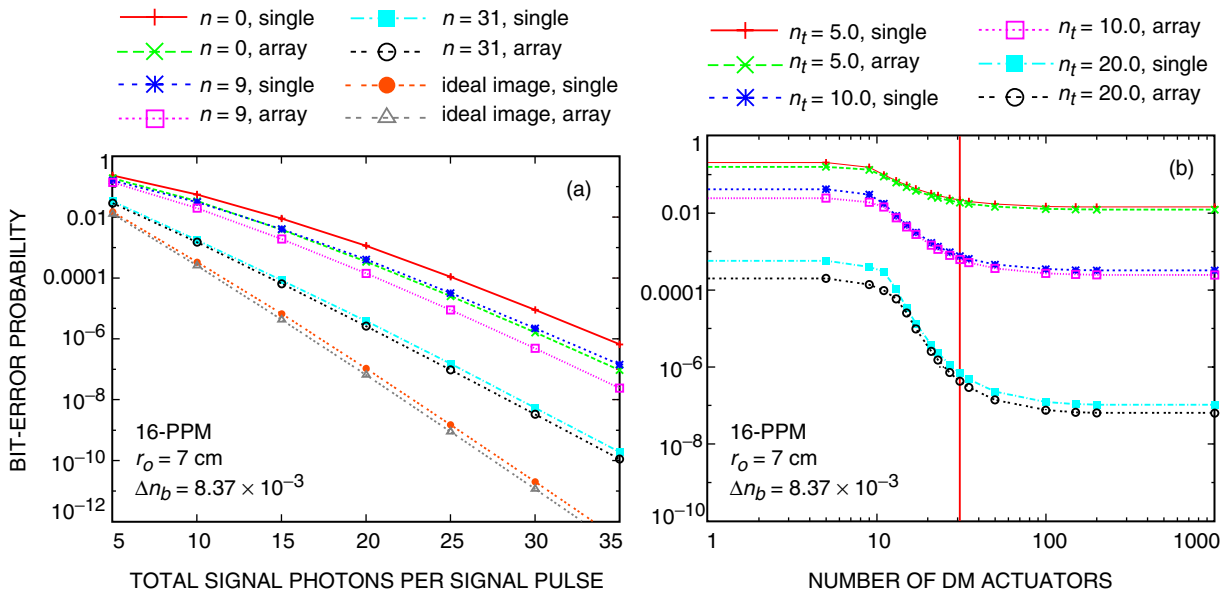

Fig. 4. Bit-error rates for an array detector and a single detector, 16-PPM, background Case (2): (a) BER versus the mean total number of detected signal photons in the focal plane for various AO systems and (b) BER versus the number of DM actuators across the pupil, for specific signal photon levels.

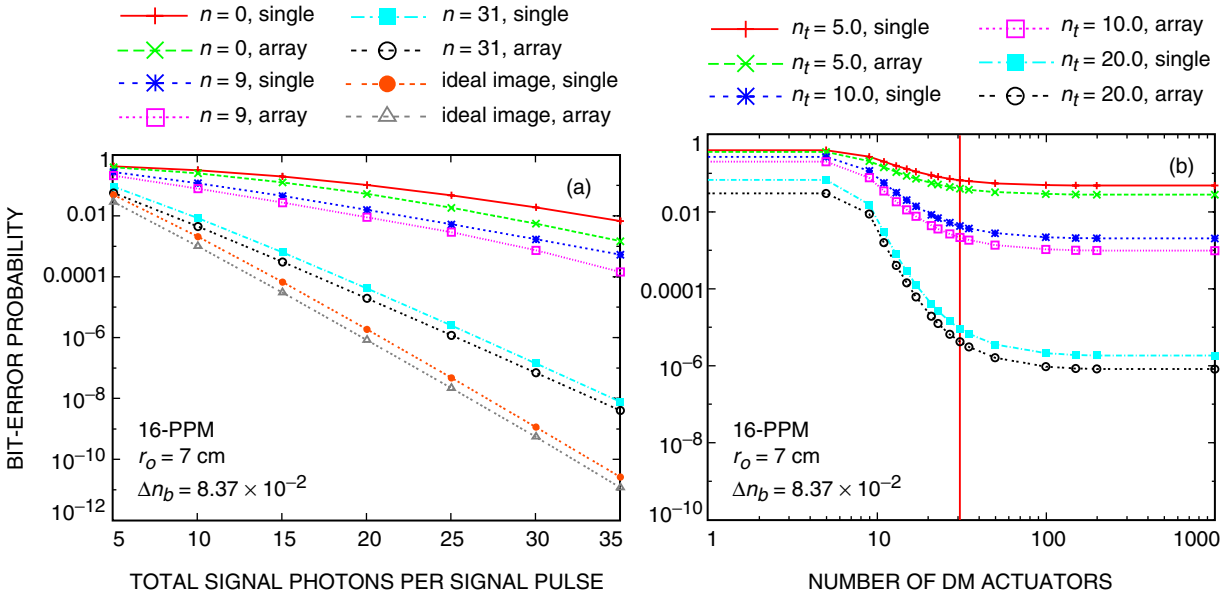

Fig. 5. Bit-error rates for an array detector and a single detector, 16-PPM, background Case (3): (a) BER versus the mean total number of detected signal photons in the focal plane for various AO systems and (b) BER versus the number of DM actuators across the pupil, for specific signal photon levels.

is greater, as the improved background-rejection capability of the array processing is of more value in this case. Figure 5 shows that, at a 0.01 BER, the $n = 31$ AO system improves performance by the considerable amount of 5.8 dB.

Figures 6 through 11 show analogous results for 64-PPM and 256-PPM, assuming the same fixed data rate of 10 Mb/s. As the PPM order increases and the data rate is fixed, the slot size decreases, resulting in less background and, consequently, smaller gains to be obtained through the use of adaptive optics.

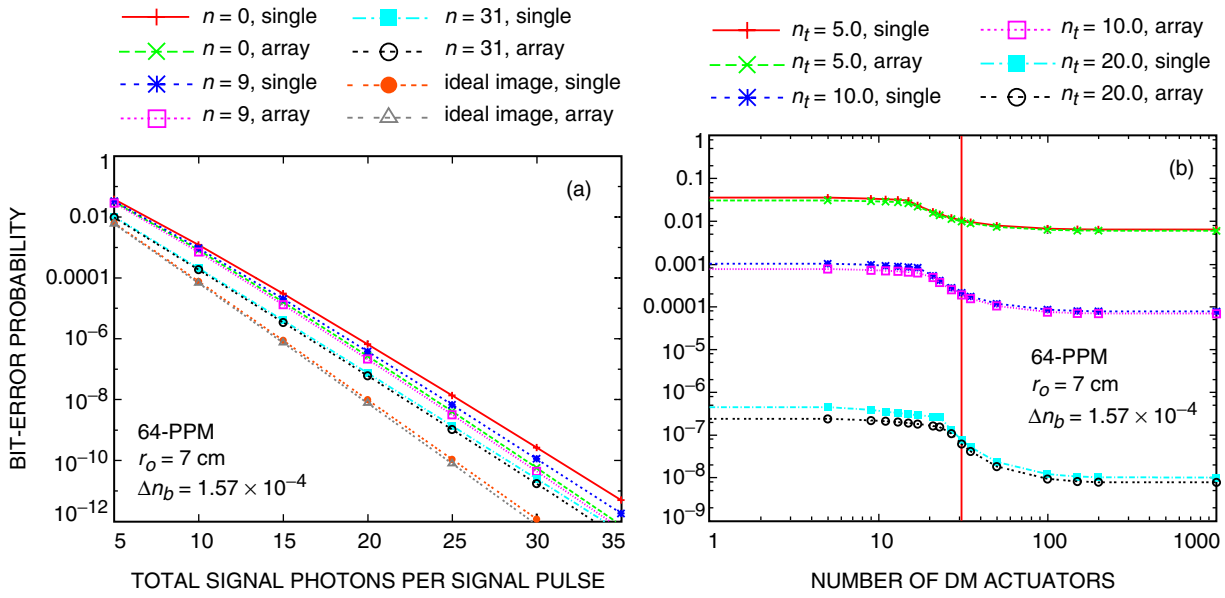

Fig. 6. Bit-error rates for an array detector and a single detector, 64-PPM, background Case (1): (a) BER versus the mean total number of detected signal photons in the focal plane for various AO systems and (b) BER versus the number of DM actuators across the pupil, for specific signal photon levels.

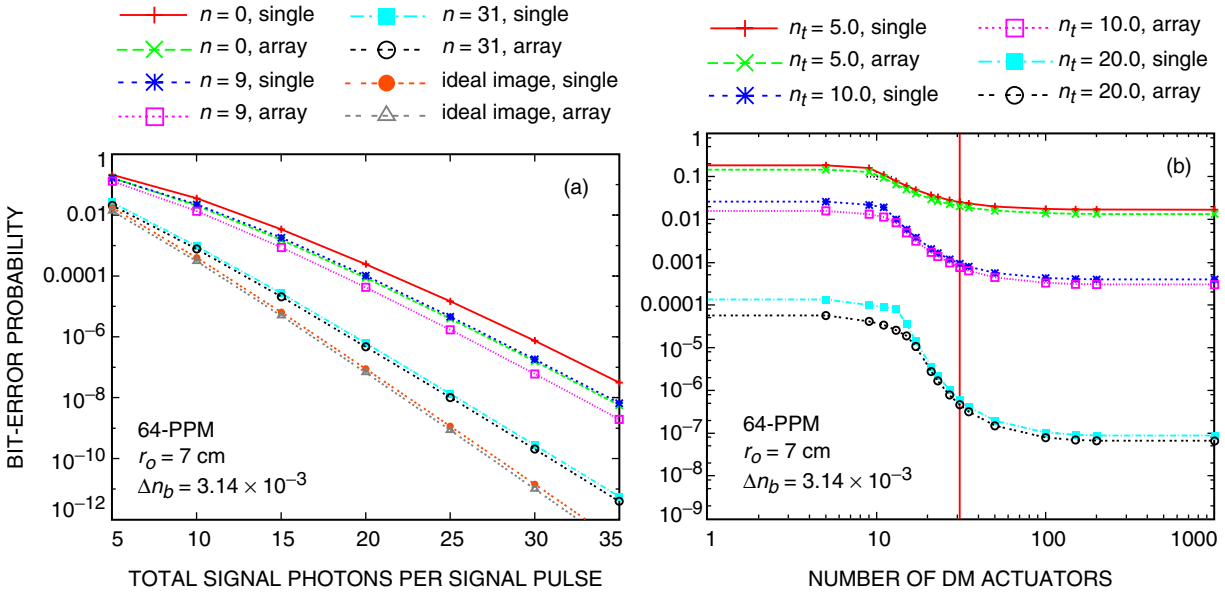

Fig. 7. Bit-error rates for an array detector and a single detector, 64-PPM, background Case (2): (a) BER versus the mean total number of detected signal photons in the focal plane for various AO systems and (b) BER versus the number of DM actuators across the pupil, for specific signal photon levels.

The results for all three modulation orders are distilled in Figs. 12 through 14, in which the gains of specific AO systems at the uncoded BER of 0.01 are charted for all three background cases. Note that while improvements as great as 3 to 6 dB are indicated for the high-background case, this background condition may occur only if direct sunlight were to strike the receiver optics, resulting in a great deal of scattered light from surface irregularities and dust. However, as indicated by the first bar in Figs. 12 and 13, improvements of 1 to 2 dB may be obtained under operating conditions in which the spacecraft is close to the Sun, and gains of 2 to 3 dB may be realized under unusual circumstances such as low-

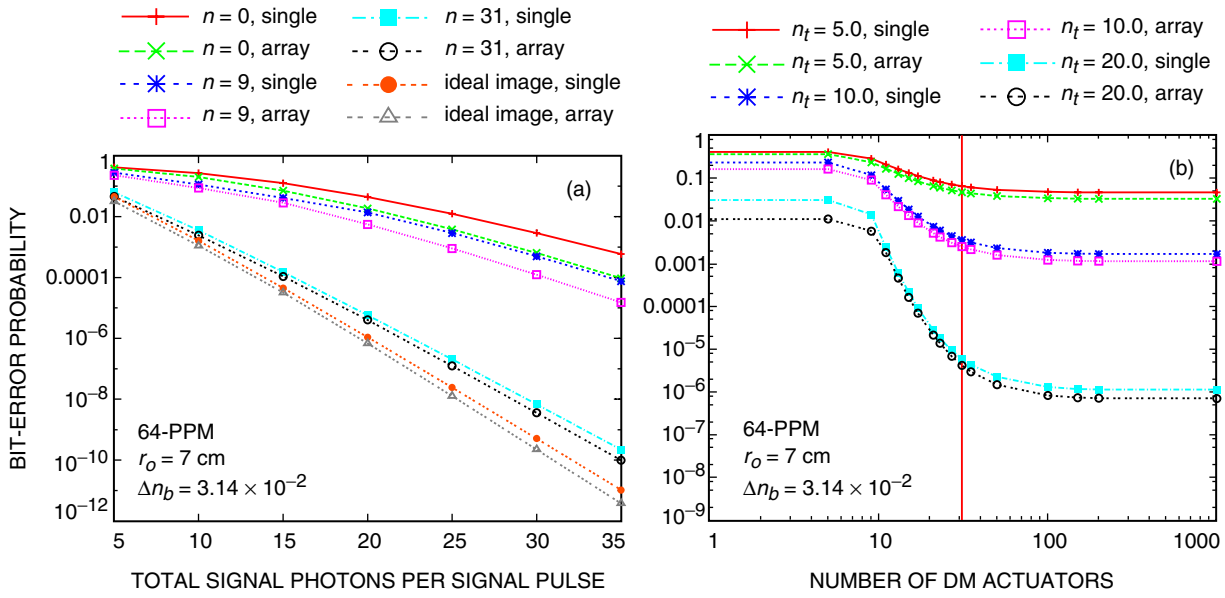

Fig. 8. Bit-error rates for an array detector and a single detector, 64-PPM, background Case (3): (a) BER versus the mean total number of detected signal photons in the focal plane for various AO systems and (b) BER versus the number of DM actuators across the pupil, for specific signal photon levels.

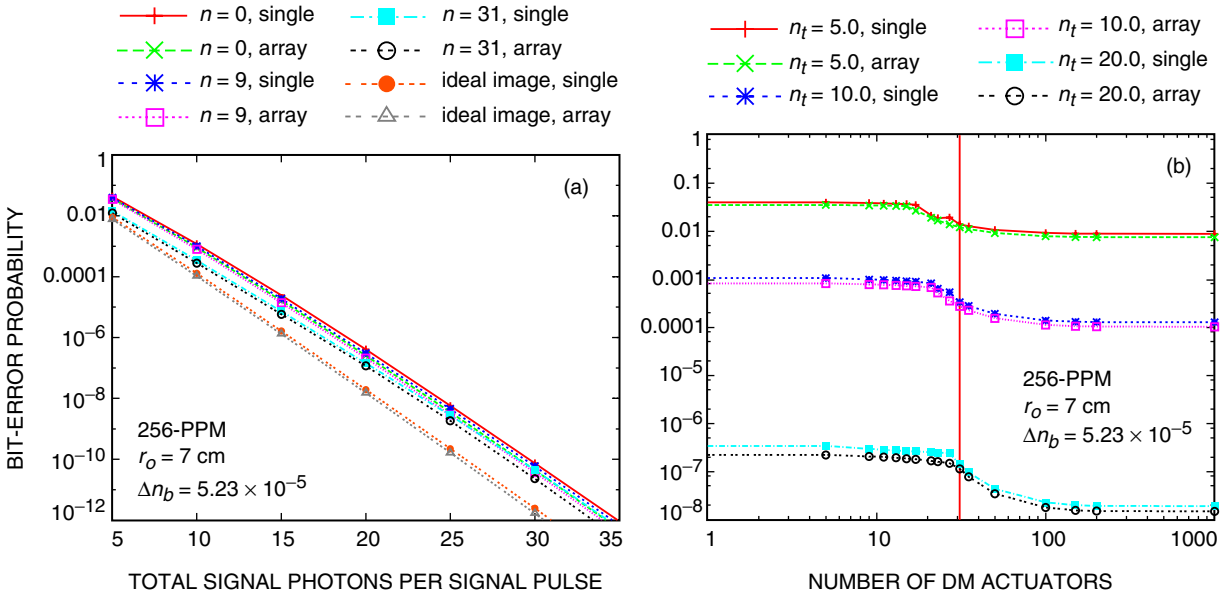

Fig. 9. Bit-error rates for an array detector and a single detector, 256-PPM, background Case (1): (a) BER versus the mean total number of detected signal photons in the focal plane for various AO systems and (b) BER versus the number of DM actuators across the pupil, for specific signal photon levels.

elevation reception close to the Sun or when looking through highly scattering light clouds, resulting in exceptionally great levels of background photons entering the receiver.

As stated earlier, a key feature of the focal-plane signal processing presented here is the ability to adaptively vary the detector size according to the signal and background conditions. AO systems with different numbers of actuators will require different detector sizes. This optimum detector size, as well as the percentage of signal energy enclosed by the optimum detector, are parameters of interest. Figure 15

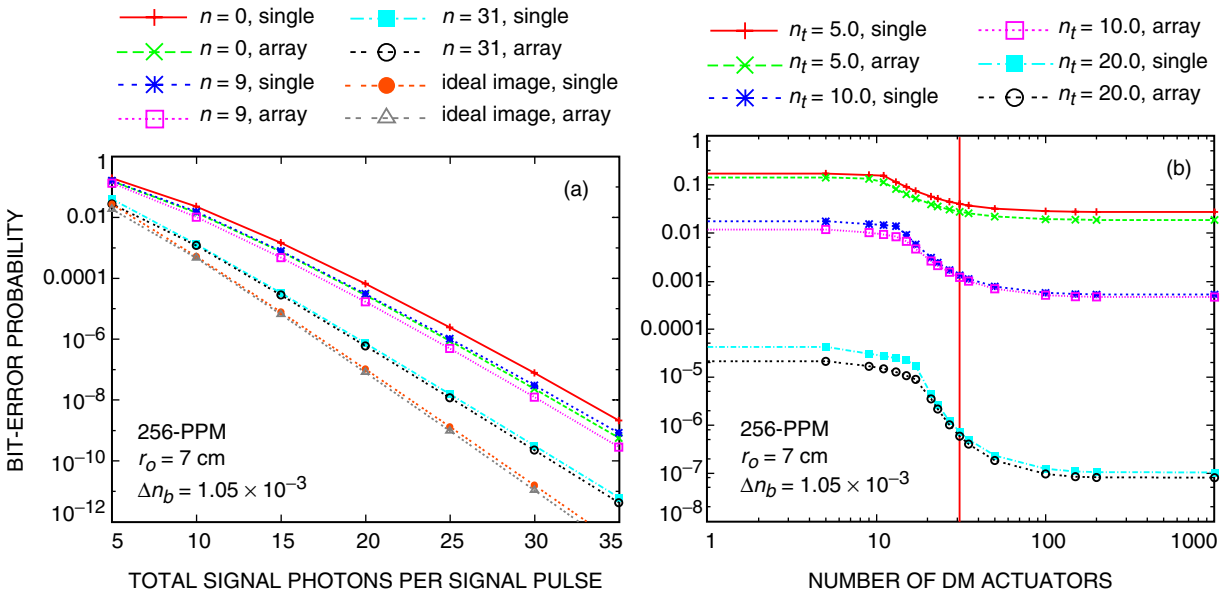

Fig. 10. Bit-error rates for an array detector and a single detector, 256-PPM, background Case (2): (a) BER versus the mean total number of detected signal photons in the focal plane for various AO systems and (b) BER versus the number of DM actuators across the pupil, for specific signal photon levels.

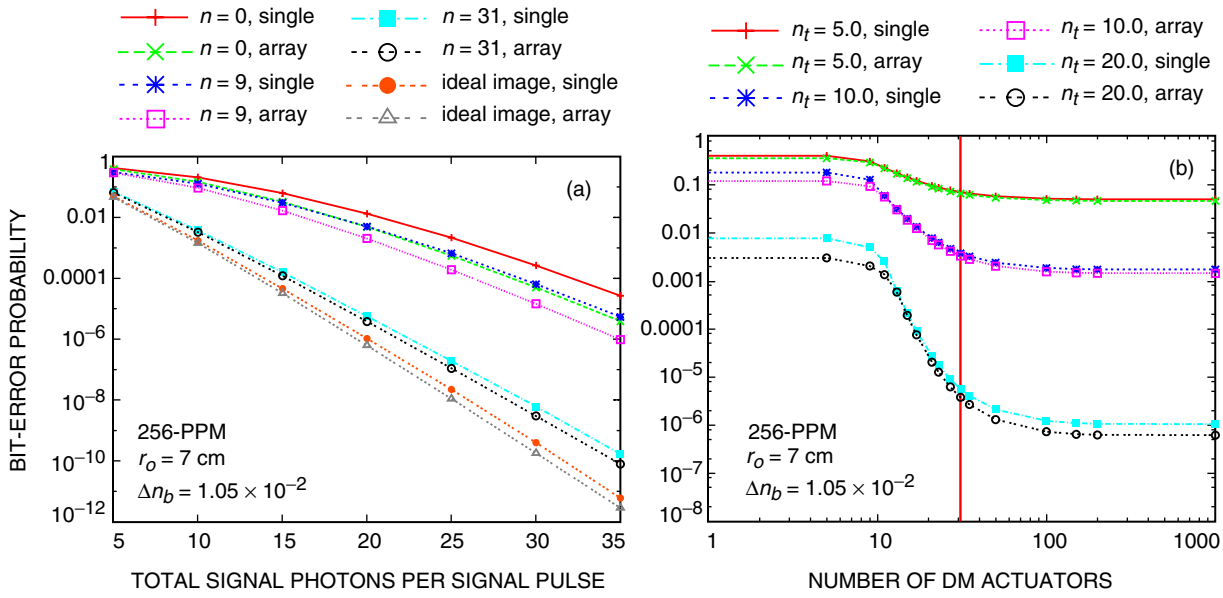

Fig. 11. Bit-error rates for an array detector and a single detector, 256-PPM, background Case (3): (a) BER versus the mean total number of detected signal photons in the focal plane for various AO systems and (b) BER versus the number of DM actuators across the pupil, for specific signal photon levels.

shows these two parameters plotted as a function of n, the number of deformable mirror (DM) actuators across the pupil. Curves are shown for the three different background levels considered in this study and 64-PPM, for both the optimized detector array and the optimally dimensioned single large detector, with the total number of signal photons fixed at $n_t = 5$. Note that the error probabilities vary for each of the points in this plot and decrease with increasing n, as given earlier in Figs. 6(b) through 8(b). In Fig. 15(a), the number of diffraction-limited elements in the non-contiguous optimal detector subarray is plotted along with the number of diffraction-limited elements in the optimally sized single detector.

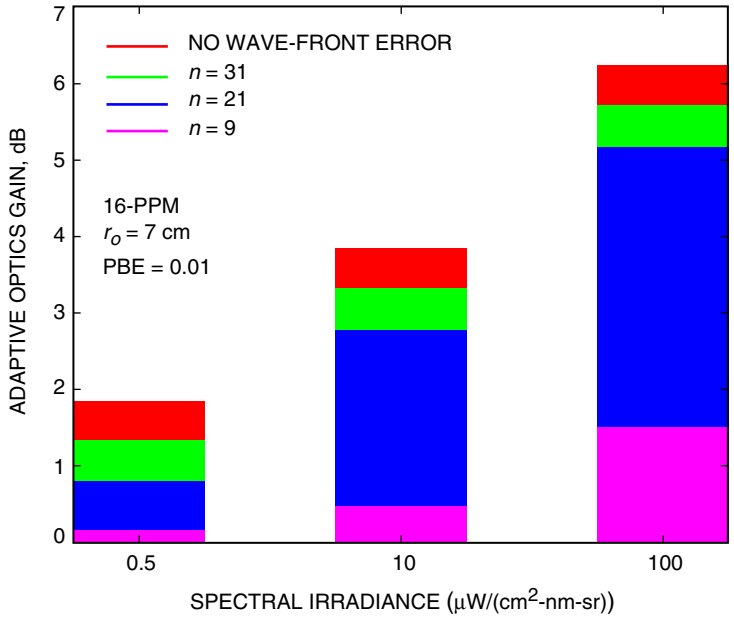

Fig. 12. Performance gains of AO systems at a 0.01 BER for 16-PPM.

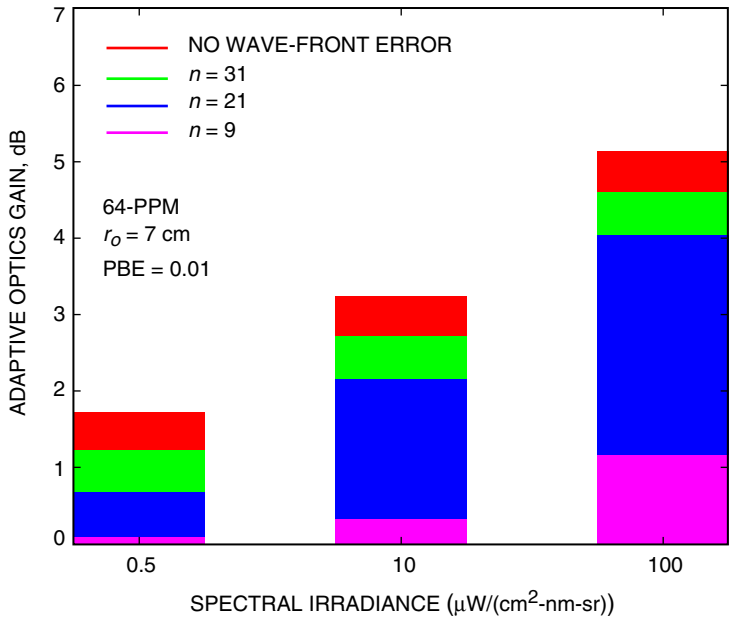

Fig. 13. Performance gains of AO systems at a 0.01 BER for 64-PPM.

Given a particular value of n, the optimum detector is larger if the background level is lower [Case (1)], and becomes smaller as the background increases. This is explained by the fact that, when the background is low, more signal energy is obtained by increasing the detector size with little penalty in increased background noise. We also observe that, for all three background levels, the optimum detector size decreases monotonically as the number of actuators in the AO system increases, with an initial constant value followed by a sharp drop with a final leveling off to a small number of elements. This reflects the effect of increasing numbers of actuators upon the focal-plane signal field: very small numbers

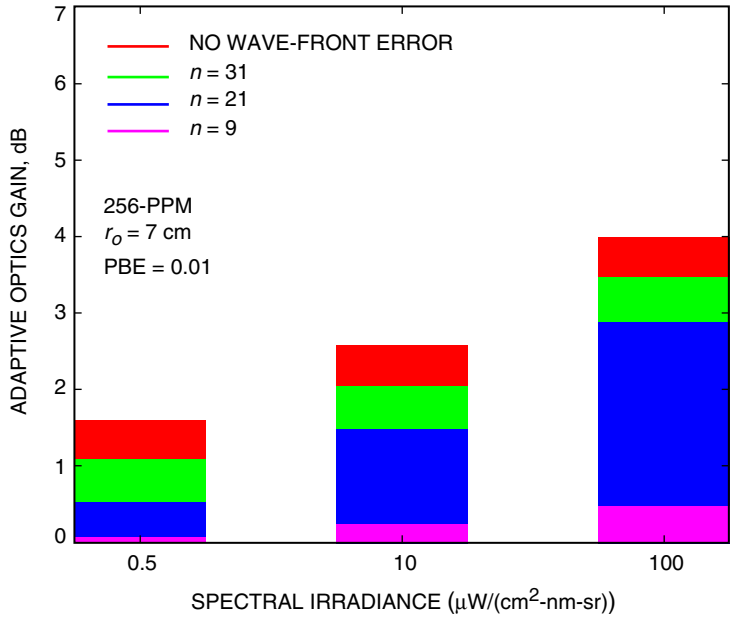

Fig. 14. Performance gains of AO systems at a 0.01 BER for 256-PPM.

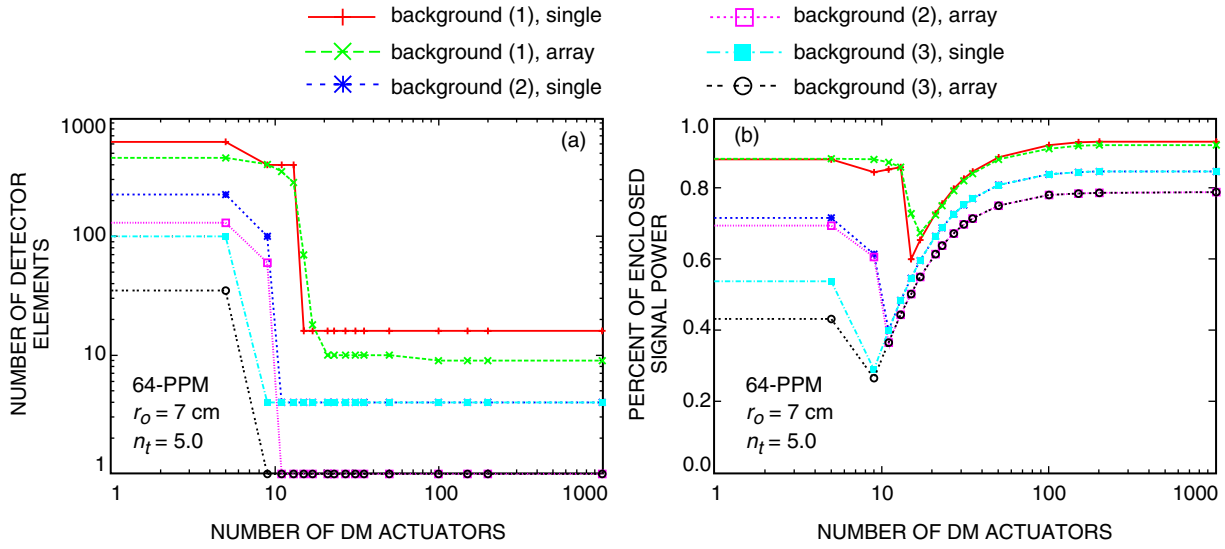

Fig. 15. For 64-PPM, $n_t = 5$ total signal photons over the entire focal plane: (a) the number of diffraction-limited focal-plane elements in the optimum detector subarray and single detector, and (b) the percentage of signal energy contained in the optimum detector array and single detector, versus the number of DM actuators across the pupil.

of actuators leave a large portion of the signal energy spread out over a large halo, requiring a larger detector size to capture it (see Fig. 1). When enough actuators are used (between 9 and 21 across the pupil), most of the signal energy is collapsed into a small area requiring only a few diffraction-limited elements. In Fig. 15(b), the actual amount of signal energy contained in the optimum detector is plotted as a percentage of $n_t = 5$ total signal photons over the entire focal-plane signal field. The behavior of these curves is somewhat interesting, with values that range between 0.43 and 0.88 for no AO and that

remain constant for low-order AO ($n = 5$ to 13, depending on the background), followed by a sharp dip to between 0.30 and 0.65, and then a gradual climb to values between 0.78 and 0.92.

The sharp dip in Fig. 15(b) may be explained by referring to Fig. 1 and considering the behavior shown in Fig. 15(a). Heuristically, we observe from Fig. 1(a) that, without AO and in the presence of turbulence, the signal energy tends to be spread over a large region in the focal plane as if the total signal energy were collected by an aperture of effective diameter r_0 (where r_0 is the Fried parameter). This means that in order to collect enough signal energy to minimize the BER in the presence of background, the receiver must open its FOV and inadvertently admit a large amount of background energy along with the signal. However, with AO compensation, a narrow core of high signal energy begins to form as the number of actuators increases, as shown in Fig. 1(b), ultimately concentrating most of the signal energy into a narrow FOV. The receiver achieves a lower BER by observing a small region around the core—equivalently, a few detector elements—containing only a fraction of the total signal energy, but at the same time rejecting most of the background energy. This occurs with different numbers of actuators in different background environments, but always leads to a sudden drop in the number of pixels that minimize BER, as can be seen in Fig. 15(a): in all three cases, there is a sudden drop in the number of detector elements observed for best performance once 10 or more actuators are employed. This explains the sudden dip in the percent of enclosed signal energy for optimum performance shown in Fig. 15(b). With the application of more actuators, the signal energy in the core increases as better AO compensation is achieved; hence, the enclosed signal energy required to minimize BER continues to increase as well, resulting in the monotonic increase in enclosed signal energy with the number of actuators after the dip in Fig. 15(b). The final values of signal energy reached under the three background conditions differ, just as the number of detector elements used for optimum performance differs, depending on the background conditions: in a high-background environment, receiver performance is dominated by the background; hence, fewer detector elements are observed in order to limit the collected background energy. With little or no background, more detector elements can be observed; hence, more signal energy is collected for best performance. In all cases, less background leads to lower error propability but requires less AO compensation.

It is important to note that the results presented here represent the gains that are achievable through the use of adaptive optics with ideal photon counting and optimized signal processing, and that issues of implementability and practically achievable gains have not been addressed. In [1], algorithms were described for suboptimal implementation of adaptive detector array processing, including estimation of signal and background levels and appropriate signal-to-noise ratio metrics for detector array element selection. While some of those techniques are applicable here, further work is necessary to identify the operating conditions under which these algorithms are practical and result in the gains described by our numerical results.

IV. Conclusions

The communications performance gains achievable through the use of adaptive optics were obtained for uncoded pulse-position modulation orders of 16, 64, and 256, for several background conditions. Through the use of Kolmogorov phase-screen atmospheric turbulence simulations and focal-plane array signal-processing algorithms, PPM bit-error probabilities were calculated, showing improvements of 1 to 2 dB in lower background conditions and gains of as much as 6 dB in very high background cases with currently realizable 1-m AO systems. Topics for further study include the extension of these results to larger apertures, understanding whether the gains demonstrated here apply directly to the coded systems, and experimental validation of the numerical results, including background levels derived from a specific mission.

References

[1] V. Vilnrotter and M. Srinivasan, "Adaptive Detector Arrays for Optical Communications Receivers," *IEEE Transactions on Communications*, vol. 50, no. 7, pp. 1091–1097, July 2002.

[2] L. C. Andrews and R. L. Phillips, *Laser Beam Propagation through Random Media*, SPIE Optical Engineering Press, Bellingham, Washington, 1998.

[3] K. Wilson, M. Troy, S. Srinivasan, B. Platt, V. Vilnrotter, M. Wright, V. Garkanian, and H. Hemmati, "Daytime Adaptive Optics for Deep Space Optical Communications," *Proceedings of 10th ISCOPS Conference*, Tokyo, Japan, December 11, 2003.

[4] P. Negrete-Regagnon, "Practical Aspects of Image Recovery by Means of the Bispectrum," *JOSA*, vol. 13, no. 7, pp. 1557–1576, July 1996.

[5] R. A. Oetjen, E. E. Bell, J. Young, and L. Eisner, "Spectral Radiance of Sky and Terrain at Wavelengths between 1 and 20 Microns. I. Instrumentation," *JOSA*, vol. 50, issue 12, pp. 1308–1312, December 1960.

[6] J. V. Sandusky, D. J. Hoppe, and M. J. Britcliffe, "Deep-Space Optical Reception Antenna (DSORA): Aperture Versus Quality," *The Telecommunications and Mission Operations Progress Report 42-143, July–September 2000*, Jet Propulsion Laboratory, Pasadena, California, pp. 1–11, November 15, 2000. http://tmo.jpl.nasa.gov/tmo/progress_report/42-143/143C.pdf